PERGAMON

Available online at www.sciencedirect.com

SCIENCE DIRECT®

Polyhedron 22 (2003) 2161–2167

POLYHEDRON

www.elsevier.com/locate/poly

Synthesis, structure and magnetism of $\{[Mn(\mu\text{-}OH)(\mu\text{-}OAc)_2]\cdot HOAc\cdot H_2O\}_n$ and the facilitation of long-range magnetic order through hydrogen bonding

David J. Price, Stuart R. Batten, Boujemaa Moubaraki, Keith S. Murray *

School of Chemistry, Monash University, P.O. Box 23, Clayton, Vic. 3800, Australia

Received 6 October 2002; accepted 23 October 2002

Abstract

The manganese(III) complex $\{[Mn(\mu\text{-}OH)(\mu\text{-}OAc)_2]\cdot HOAc\cdot H_2O\}_n$ (**1**·HOAc·H_2O) has a structure in which linear chains, containing three bridges made up of one hydroxide and two acetates, are linked together by hydrogen bonds to form 2D sheets. These hydrogen bonds exist between the μ-OH^-, the solvated acetic acid and water molecules, and the μ-OAc^- ligands on adjacent chains. The complex has particularly interesting magnetic properties that include weak intra-chain antiferromagnetic coupling at higher temperatures and a magnetic phase transition, at $T_N = 6.1$ K, to an ordered antiferromagnetic phase. This ordering is probably brought about by the hydrogen-bonding pathways joining the chains. Removal of water and acetic acid solvate molecules results in the loss of the long-range order. Detailed DC and AC magnetization studies, made over a wide range of applied magnetic fields and temperatures, show that below T_N, there is a metamagnetic transition at approximately 1000 Oe, brought about by increasing the applied fields, from the antiferromagnetic phase to a canted-spin antiferromagnetic (weak ferromagnetic) phase.

Keywords: Manganese(III); Carboxylate chain structures; Hydrogen-bonded sheets; Metamagnetism; Crystal structures

1. Introduction

Studies of covalent ligand bridging in extended network coordination polymers and how this influences magnetic coupling and long-range order have increased enormously in recent years. The bridging groups CN^-, $C_2O_4^{2-}$, RCO_2^- [1–6] and poly-cyano ligands such as $N(CN)_2^-$ [7–9] have received most attention. Less well studied, however, is magnetic order occurring via hydrogen-bonding pathways, but this is a growing field within supramolecular magnetochemistry, and a number of examples have been discovered recently [10–13]. Generally, the J values and T_C (or T_N) values in such systems are very low with the ordering temperatures less than 10 K. However, we have noted a T_C value of 23 K in a heterobimetallic Ni_3Fe_2 cluster system in which well-ordered hydrogen-bonded $(H_2O)_7$ arrays join the clusters [14].

We describe here a new polymeric carboxylate-bridged complex, $\{[Mn(\mu\text{-}OH)(\mu\text{-}OAc)_2]\cdot HOAc\cdot H_2O\}_n$ (**1**·HOAc·H_2O), which displays long-range antiferromagnetic order ($T_N = 6.1$ K) facilitated by hydrogen bonding, together with a field-induced metamagnetic transition. The desolvated material, **1**, does not order magnetically. The solvated complex was discovered during attempts to link Mn_3 and Mn_4 carboxylate cluster complexes with pseudo-halide ligands, in this case dicyanonitrosomethanide ($ONC(CN)_2^-$, $dcnm^-$), to form extended networks of clusters. The $dcnm^-$ group was not contained in the product. Similar work with dicyanamide ($N(CN)_2^-$) recently led to the simultaneous discovery of a large manganese(III/IV) carboxylate-alkoxo cluster, $[Mn_{16}O_{16}(OMe)_6(OAc)_{16}(MeOH)_3(H_2O)_3]\cdot 6H_2O$, which is a new example of a single molecule magnet (SMM), and a linear chain Mn^{III}

* Corresponding author. Tel.: +61-3-9905-4512; fax: +61-3-9905-4597.

E-mail address: keith.s.murray@sci.monash.edu.au (K. Murray).

0277-5387/03/$ - see front matter
doi:10.1016/S0277-5387(03)00180-3

complex $\{[Mn(\mu\text{-}OMe)(\mu\text{-}OAc)_2]\}_n$ [15]. Again, the $N(CN)_2^-$ ligand was not present in the products.

2. Experimental

$Mn(OAc)_2\cdot 4H_2O$, acetonitrile, ethanol and glacial acetic acid were used as received. All reactions were performed under aerobic conditions. $Me_4N(dcnm)$ was prepared by a metathesis reaction by adding an acetonitrile solution of Me_4NBr to a suspension of Ag(dcnm) in dichloromethane ($dcnm^-$ is $ONC(CN)_2^-$). AgBr was removed by filtration. The solvent was removed and the resulting yellow oil was recrystallized by vapour diffusion of diethyl ether into a solution in methanol (yield 95%). Ag(dcnm) [16] and $n\text{-}Bu_4NMnO_4$ [17] were prepared according to the literature. *Warning:* Extreme caution should be taken in the use of organic permanganates.

2.1. Synthesis

An ethanolic solution (10 ml) of $Me_4N(dcnm)$ (0.195 g, 1.16 mmol) was added with stirring to a solution of $Mn(OAc)_2\cdot 4H_2O$ (0.284 g, 1.16 mmol) in 10 ml acetonitrile, 20 ml ethanol and 7 ml glacial acetic acid. Then, solid $n\text{-}Bu_4NMnO_4$ (0.076 g, 0.210 mmol) was added in small portions. At this time, the solution was a dark red/brown colour. The solution was stirred for about 3 h, after which a small amount of the solution was placed in a Petrie dish to evaporate, and the remainder was covered and left to stand. After 1 day, many red-orange crystals had formed. These were collected by filtration, washed with ethanol and dried with ether and placed under nitrogen to prevent desolvation that occurred in air over a period of days (yield ~90 mg, 21% based on total available Mn). Infrared spectrum (Nujol mull, cm^{-1}): 3336sbr, 2601vw, 2040vw, 1776vw, 1699s, 1505s, 1455s, 1277s, 1148m, 1039m, 963vw, 888w, 676w. Microanalysis (%) found: C, 26.8; H, 4.7; N, nil. Calc. for $C_6H_{13}MnO_8$: C, 26.9; H, 4.9%.

After about 1 week, many red-orange crystals and rod-like crystals were present in the remaining solution. A suitable crystal was chosen for a single-crystal X-ray diffraction experiment.

It was subsequently found that $Me_4N(dcnm)$ was not necessary for the successful synthesis of $\mathbf{1}\cdot HOAc\cdot H_2O$. Thus, solid $n\text{-}Bu_4NMnO_4$ (0.076 g, 0.210 mmol) was added in small portions with stirring to a solution of $Mn(OAc)_2\cdot 4H_2O$ (0.284 g, 1.16 mmol) in 10 ml acetonitrile, 20 ml ethanol and 7 ml glacial acetic acid. The resultant dark black-brown solution was left to stand to slowly evaporate. After several months, the solution (now colourless) had almost evaporated to dryness and a solid was present consisting of red-orange needles. About half of this solid was collected by filtration, washed quickly with ethanol, dried with ether, then placed under nitrogen (yield 0.076 g, 21% based on total available Mn). Infrared spectrum (Nujol mull, cm^{-1}): 3326sbr, 1700s, 1538s, 1438s, 1278m, 1150m, 1038m, 888w. Microanalysis (%) found: C, 27.0; H, 4.8; N, nil. Calc. for $C_6H_{13}MnO_8$: C, 26.9; H, 4.9%.

2.2. X-ray crystallographic studies

Crystal data for $\mathbf{1}\cdot HOAc\cdot H_2O$ are summarized in Table 1. Data were collected on a dichroic yellow-red rod-like crystal using a Nonius KappaCCD diffractometer with graphite monochromated Mo Kα radiation ($\lambda = 0.71073$ Å). Integration was carried out by the program DENZO-SMN [18], and data were corrected for Lorentz polarization effects and for absorption using the program SCALEPACK [18]. Further, face-indexed absorption corrections were applied. Solutions were obtained by direct methods (SHELXS 97) [19] followed by successive Fourier difference methods, and refined by full-matrix least-squares on F_{obs}^2 (SHELXL 97). All non-hydrogen atoms were refined anisotropically. The hydrogen atoms of the chain, the oxygen-bound acetic acid hydrogen atom and the water hydrogen atom were located and refined isotropically and their bond lengths were restrained using the DFIX command to be 0.96(2) and 0.90(2) Å for the carbon- and oxygen-bound hydrogens, respectively. The methyl hydrogen atoms of the acetic acid were not included due to the large

Table 1
Summary of crystal data

	$\mathbf{1}\cdot HOAc\cdot H_2O$
Empirical formula	$C_6H_{13}MnO_8$
M	268.10
Crystal system	monoclinic
Space group	$P2_1/m$
a (Å)	7.9134(2)
b (Å)	6.7648(2)
c (Å)	10.8644(3)
β (°)	106.90(1)
U (Å^3)	556.48(3)
Z	2
T (K)	123(2)
μ(Mo Kα) (mm^{-1})	1.207
Crystal dimensions (mm)	0.22 × 0.03 × 0.03
Index ranges	$-10 \le h \le 9$, $-9 \le k \le 7$, $-14 \le l \le 14$
Completeness to $2\theta = 55°$ (%)	99.8
Data collected	4528
Unique data (R_{int})	1482 (0.0437)
Observed reflections [$I > 2\sigma(I)$]	1224
Parameters	109
Final R_1, wR_2 [$I > 2\sigma(I)$] [a]	0.0329, 0.0835
All data	0.0433, 0.0883
Goodness of fit, S	1.081

[a] $R_1 = \Sigma||F_o|-|F_c||/\Sigma|F_o|$, $wR_2 = \{\Sigma[w(F_o^2-F_c^2)^2]/\Sigma[w(F_o^2)^2]\}^{1/2}$.

thermal motion of the methyl carbon (refinements of such hydrogen atoms presented extremely large U_{iso} values) and their relative unimportance with respect to the hydrogen-bonding interactions.

2.3. Thermogravimetric studies

Thermal degradation studies were performed on a Simultaneous Thermal Analyzer (Rheometric Scientific, STA 1500), which was calibrated using a four-point melt series (indium, tin, lead and zinc). Experiments were performed in aluminium pans. Three freshly prepared samples of **1**·HOAc·H_2O were used. Two experiments were performed under a N_2 flow, between 25 and 400 °C with heating rates of 2 and 10 °C min^{-1}. One experiment was performed under a flow of dried air, between 25 and 150 °C with a heating rate of 0.5 °C min^{-1}. A mass loss of 27–28% occurred up to 80 °C, and the calculated value of loss of HOAc·H_2O being 29.1%.

2.4. Magnetic studies

The instrumentation (Quantum Design MPMS 5 and PPMS (AC)), DC magnetization and AC susceptibility protocols have been described previously [7]. Care was taken to see that **1**·HOAc·H_2O did not partially desolvate in the sample chamber and it was found that use of a gelatine capsule to contain the sample was adequate.

3. Results and discussion

3.1. Synthesis and characterization

Reaction of n-Bu_4NMnO_4 with a solution of $Mn(OAc)_2·4H_2O$ ($\sim$1:5 molar ratio) in acetonitrile/ethanol/glacial acetic acid gave a dark brown solution. After several months of slow evaporation, the solution had become colourless and red-orange needles of **1**·HOAc·H_2O are formed. The infrared spectrum of these crystals shows ν(OH) at 3326 cm^{-1}. This peak is relatively sharp due to the presence of hydrogen bonding of both the μ-OH and the lattice water. The absorption at 1700 cm^{-1} is probably due to the δ(HOH) vibration of the lattice water. The strong absorption at 1538 cm^{-1} is due to the ν(C=O) vibrations of the bridging acetates and lattice acetic acid. The microanalyses for two successfully prepared samples were consistent with the formulation of **1**·HOAc·H_2O. The first method employed, which was actually aimed to incorporate the bridging ligand $dcnm^-$, is described in Section 2. It gave crystals within 1 week. TGA studies showed that the acetic acid and water molecules can be removed to yield **1**.

3.2. Crystal structure

Complex **1**·HOAc·H_2O crystallizes in the monoclinic space group $P2_1/m$. Table 2 contains selected bond distances and angles. The asymmetric unit contains half a manganese(III) ion, two half acetates, one half hydroxide, acetic acid and water. The metal lies on an inversion centre whereas all other groups lie on the same mirror plane (excluding the oxygens and two of the hydrogen atoms of the acetates and the water hydrogen). As seen in Fig. 1, the crystal structure consists of chains of manganese(III) ions bridged by single μ-OH^- and double μ-OAc^- bridges. These chains run parallel to the b-axis direction. A network of hydrogen bonding exists between each adjacent chain in the ab-plane that involves the μ-OH^-, the lattice acetic acid and water molecules. This results in hydrogen-bonded sheets that stack parallel to the c-axis direction. The coordination environment of each Mn^{III} atom is Jahn-Teller elongated as expected for a near-octahedral d^4 ion. The equatorial plane contains the shortest coordination bond, which is to the μ-OH^- oxygen (Mn(1)–O(8) = 1.8993(8) Å), and also contains one of the μ-OAc^- ligand oxygen atoms (Mn(1)–O(5) = 1.939(1) Å). The remaining two equatorial sites are filled by the two symmetry equivalents of these atoms. The other μ-OAc^- ligand oxygen atom and its symmetry equivalent occupy the elongated axial sites (Mn(1)–O(2) = 2.179(1) Å). The intra-chain Mn···Mn distance, 3.3824(2) Å, is equal to half the unit cell length b. Similarly, the shortest inter-chain Mn···Mn distance within the hydrogen-bonded sheets, 7.9134(2) Å, is equal to the unit cell length a. The lattice acetic acid molecule was assigned as

Table 2
Selected interatomic distances (Å) and angles (°)

Mn(1)–O(2)	2.179(1)	Mn(1)–O(8)	1.8993(8)
Mn(1)–O(5)	1.939(1)	Mn(1)···Mn(1 [a])	3.3824(2)
O(2)–Mn(1)–O(5)	91.54(6)	O(2)–Mn(1)–O(5 [b])	88.46(6)
O(2)–Mn(1)–O(8)	92.69(6)	O(2)–Mn(1)–O(8 [b])	87.31(6)
O(5)–Mn(1)–O(8)	92.16(6)	O(5)–Mn(1)–O(8 [b])	87.84(6)
Hydrogen bonds			
O(8)–H(8)	0.89(2)	O(12)–H(12)	0.90(2)
H(8)···O(9)	1.82(2)	H(12)···O(13)	1.66(2)
O(8)···O(9)	2.691(3)	O(12)···O(13)	2.550(3)
O(13)–H(13)	0.92(2)		
H(13)···O(2 [c])	1.85(2)		
O(13)···O(2 [c])	2.759(2)		
O(8)–H(8)···O(9)	166(4)	O(12)–H(12)···O(13)	170(8)
O(13)–H(13)···O(2 [c])	171(3)		

[a] Symmetry transformation: $1-x$, $1/2+y$, $-z$.
[b] Symmetry transformation: $-x+1$, $-y$, $-z$.
[c] Symmetry transformation: $-x+2$, $-y$, $-z$.

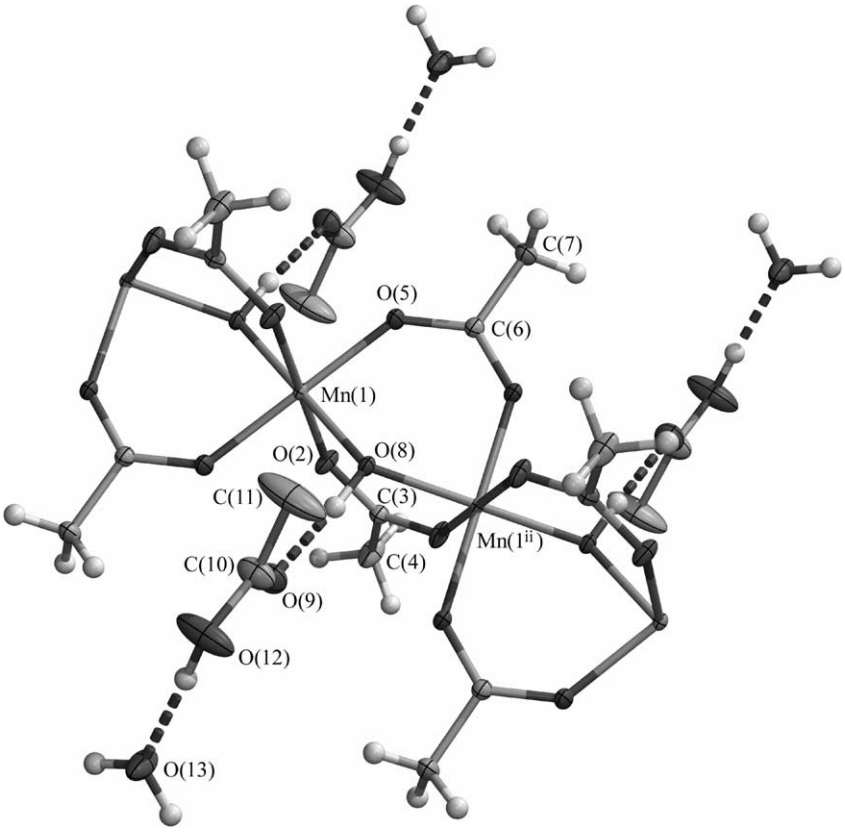

Fig. 1. Crystal structure of $\{[Mn(OH)(OAc)_2]\cdot HOAc\cdot H_2O\}_n$ ($\mathbf{1}\cdot HOAc\cdot H_2O$) with atom labelling scheme (thermal ellipsoids shown at 50% probability).

such rather than a free acetate ion for a number of reasons. The manganese ion was assigned as Mn^{III} from coordination bond distance and Jahn-Teller distortion considerations and thus charge balance is obtained by the μ-OH^- and the two μ-OAc^- bridging ligands. One of the C–O bond distances (C(10)–O(9) = 1.191(4) Å) of the acetic acid molecule is consistent with a carbonyl bond and the other (C(10)–O(12) = 1.316(4) Å) is likewise consistent with a single C–O bond. Finally, a proton was found on O(12) in the direction of the lattice water, O(13), further indicating it to be a molecule of acetic acid.

The hydrogen-bonding network between chains occurs via the following pathway. The μ-OH^- hydrogen bonds to the carbonyl oxygen atom of the lattice acetic acid molecule (O(8)···O(9) = 2.691(3) Å). The acetic acid then hydrogen bonds to the lattice water (O(12)···O(13) = 2.550(3) Å) which is in turn hydrogen-bonded to two acetate oxygen atoms on two μ-OAc^- ligands on the adjacent chain (O(13)···O(2^a) = 2.759(2) Å, where a: −x+2, −y, −z). The shortest inter-sheet Mn···Mn distance, 10.8644(3) Å, is equal to the unit cell length *c*. Fig. 2 shows two such hydrogen-bonded sheets.

3.3. Magnetism

Two samples were investigated and gave identical results. In a field of 1 T, the magnetic moment of $\mathbf{1}\cdot HOAc\cdot H_2O$ decreases gradually from 4.7μ_B ($\chi T = 2.76$ cm^3 mol^{-1} K) at 300 K to 2.9μ_B ($\chi T = 1.05$ cm^3 mol^{-1} K) at ~12 K, then it increases to yield a sharp maximum at ~8 K of 3.5μ_B ($\chi T = 1.53$ cm^3 mol^{-1} K) before decreasing to reach 1.9μ_B at 2 K ($\chi T = 0.45$ cm^3 mol^{-1} K) (Fig. 3). The 12–300 K region shows a corresponding Curie–Weiss behaviour with $\theta = -27$ K and $C = 2.8$ cm^3 mol^{-1} K. This is indicative of intra-chain antiferromagnetic coupling. When the sample is desolvated by heating at 80 °C in vacuo, the sharp transition at 12 K disappears and the moments decrease more quickly than in the parent solvate, from 4.6μ_B ($\chi T = 2.65$ cm^3 mol^{-1} K) at 300 K to 1.25μ_B ($\chi T = 0.195$ cm^3 mol^{-1} K) at 2 K. The corresponding χ_{Mn} values show Curie–Weiss behaviour, without a maximum, which indicates very weak coupling and/or monomer impurity being present which shows a maximum in χ_{Mn}. These differences in behaviour show that intra-chain antiferromagnetic coupling persists in the desolvated species and that a magnetic phase transition

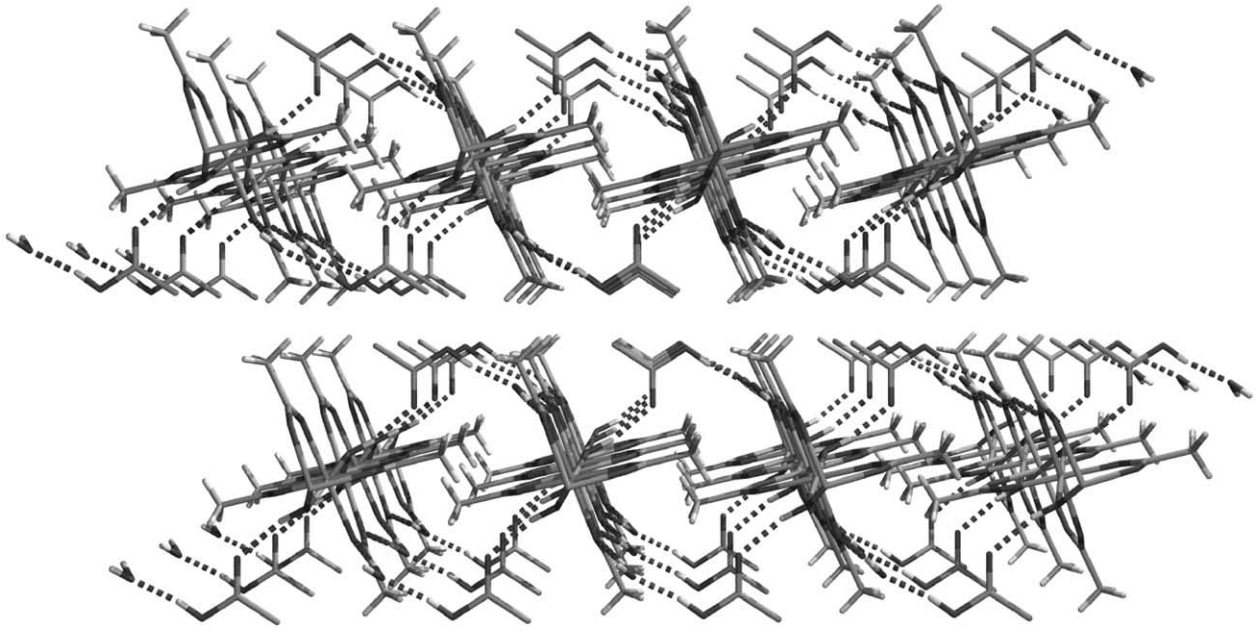

Fig. 2. Packing diagram of $\{[Mn(OH)(OAc)_2]\cdot HOAc\cdot H_2O\}_n$ (**1**·HOAc·H_2O) showing hydrogen-bonded chains forming sheets.

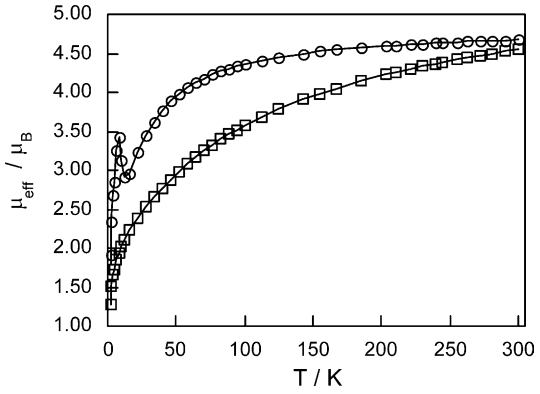

Fig. 3. Plots of effective magnetic moment, μ_{Mn} ($=2.83\sqrt{\chi T}$), versus temperature in a field of 1 T for **1**·HOAc·H_2O (○) and the desolvated species, **1** (□) (in these and other magnetic plots, the solid lines are not calculated fits).

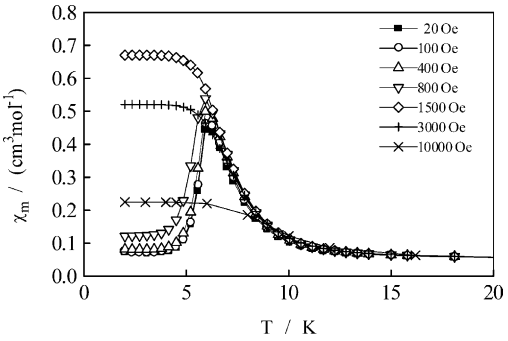

Fig. 4. Temperature dependence of the DC magnetic susceptibilities for **1**·HOAc·H_2O in the applied fields shown.

to an ordered state below ~12 K occurs in **1**·HOAc·H_2O; it is likely that the hydrogen-bonded pathways between the chains are responsible for long-range order but this cannot be proven unambiguously.

A range of magnetic measurements was employed to probe the nature of the long-range order in **1**·HOAc·H_2O. First, the use of lower fields in the DC susceptibility measurements (20, 100, 400, 800 Oe) confirmed the sharp maximum in χ_{Mn} at 6.0 K in these fields, with χ_{max} moving only a little to lower temperature and increasing only a little in value when applied fields of 20–800 Oe were progressively used (Fig. 4). The T_N value of 6.1 K was confirmed from plots of $d(\chi T)/dT$ versus T. The shape of the sharp maxima in χ_{Mn} is indicative of long-range antiferromagnetic order occurring although extrapolation of the χ_{Mn} values to 0 K, below χ_{max}, in a field of 20 Oe, is close to 1/6 of the value at χ_{max} (T_N) rather than the 2/3(χ_{max}) expected for a two sub-lattice collinear-antiferromagnet. Kurmoo and co-workers [20] have observed similar ratio values in Co^{II} carboxylate materials. It is possible that orientation of crystallites is occurring giving χ''-like behaviour, a phenomenon known in anisotropic Mn^{III} species [21]. Use of a 1500-Oe field showed no maximum but a saturation in χ_{Mn} below ~4 K. The 3000 Oe field data behaved likewise, but the saturation χ value was lower than in the 1500 Oe field and lower again in the 1 T field. This field-dependent behaviour in the 20–1500 Oe region is indicative of either spin-flop behaviour observed in weakly coupled antiferromagnets [12,22–24] or, more likely, of metamagnetic behaviour in which a ferromagnetic phase is induced by increasing the applied field. In the present case, the high-temperature region (10–300 K) displays antiferromagnetic coupling and thus, if metamagnetism occurs, a ferromagnetic phase

must be of the weak ferromagnet/canted-spin antiferromagnet type. The decrease observed in the saturation value of χ, at temperatures below 6 K, as H is increased from 1500 to 3000 and 10,000 Oe is a result of the canted-spin antiferromagnetism that will align spins opposite to the field. Indeed, this can be seen in the magnetization isotherms shown in Fig. 5 which, at 2, 3 and 4 K, show sigmoidal M versus H behaviour typical of metamagnetism (critical field ≈ 1000 Oe), while at higher fields, e.g. 3000, 10,000 Oe, the χ (from M/H) values at 2–5 K are lower than at 1500 Oe because of the spin-canting. The M values increase slowly, and almost linearly, between 1 and 5 T (below T_N), reaching $0.79N\beta$ at $H = 5$ T (not shown in Fig. 5 for clarity), a value well below the $S = 2$ value of $4N\beta$. Presumably, an enormous field would be required to reach saturation and a ferromagnetic phase. This contrasts with the rapid change from antiferromagnetic to canted-spin phase in small, increasing fields. Recent examples of somewhat similar but not identical field-induced antiferromagnetic to canted-spin antiferromagnetic or to ferromagnetic transitions have been given by Kurmoo and co-workers [20] and by Mallah and co-workers [25] for a 2D Co^{II}-pyromellitate and a 2D $Cr^{III}Ni^{II}$ cyano-bridged system, respectively.

The present compound shows essentially no hysteresis in M, at 2 K, in the ± 2000 Oe DC sweep (Fig. 6), the sigmoidal behaviour being clearly evident. The in-phase AC susceptibility component, χ', measured using a field of 10 Oe and frequency of 100 Hz, shows a sharp maximum at 6.2 K and a shoulder at 3.9 K, while the out-of-phase component χ'', shows zero at 6.2 K but, surprisingly a sharp maximum at 2.3 K (Fig. 7). These data also support antiferromagnetic order occurring below 6.2 K, the transition at 2.3 K probably being due to the spin-canting.

Measurement of the field-cooled magnetization (FCM), $H = 10$ Oe, and the zero-field-cooled magnetization (ZFCM) show identical behaviour at temperatures 4–25 K with a sharp maximum at 6.1 K and the

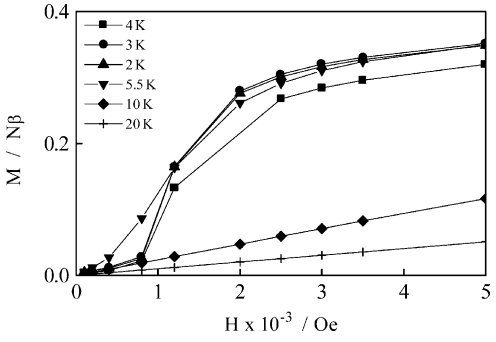

Fig. 5. Isothermal magnetization of $\mathbf{1}\cdot HOAc\cdot H_2O$ at 2 K (▲), 3 K (●), 4 K (■), 5.5 K (▼), 10 K (◆) and 20 K (+). Note that at 2 K, the M values have close to linear dependence on H up to 5 T and do not saturate (see text).

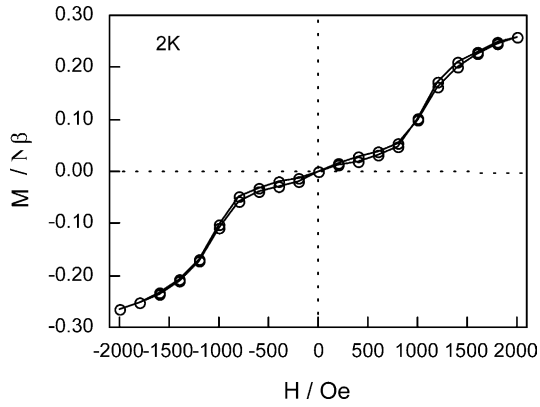

Fig. 6. Isothermal magnetization of $\mathbf{1}\cdot HOAc\cdot H_2O$ at 2 K in the field ranges of ± 2000 Oe.

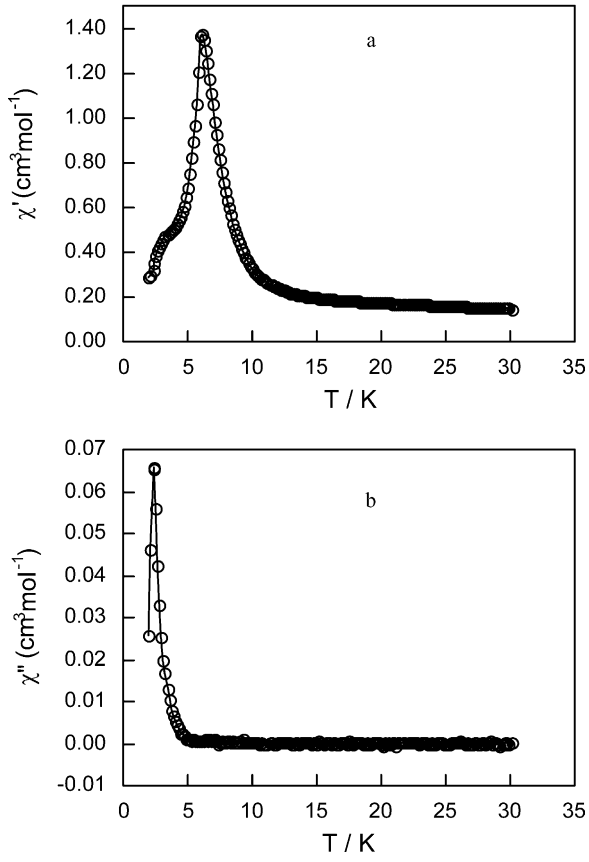

Fig. 7. (a) Temperature dependence of AC in-phase magnetic susceptibility, χ', in a field of 10 Oe and frequency of 100 Hz and (b) temperature dependence of AC out-of-phase component, χ''.

cusp-like decrease in M, below T_N (Fig. 8). The lack of any bifurcation of FCM and ZFCM plots is indicative of being in an antiferromagnetic phase in this 10 Oe field. Canted-spin antiferromagnets or ferromagnets would show bifurcation at T_C and would show hysteresis. Future work will involve measurements in the 2–4 K region.

In summary, the magnetic data for the layered structure in $\mathbf{1}\cdot HOAc\cdot H_2O$ are compatible with the

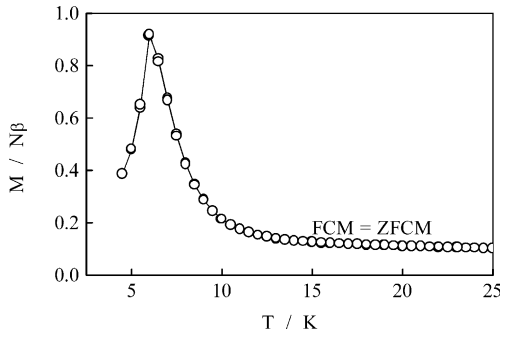

Fig. 8. Temperature dependence (4–25 K) of FCM and ZFCM for **1**·HOAc·H_2O.

occurrence of weak antiferromagnetic coupling along the Mn^{III} chains mediated by two μ-OAc^- and one μ-OH^- bridges, as often is the case in similarly tri-bridged dinuclear Mn^{III} complexes [26]. Long-range antiferromagnetic order occurs below a T_N of 6.1 K probably involving hydrogen-bonded (Mn–OH···HO_2CCH_3···OH_2···O_2CCH_3–Mn) pathways between the chains. An unusual antiferromagnetic to canted-spin antiferromagnetic (weak ferromagnetic) transition occurs as the field is raised from 0 to approximately 1000 Oe, the spin-canting originating from chain–chain interactions containing anisotropic Mn^{III} centres. Removal of the solvate molecules removes the 3D magnetic order. There are other recent examples of hydrogen-bonded networks having ordering temperatures of similar magnitude to that observed here [10–13]. In one such example of a {Ni^{II}alcohol-nitroxyl radical} heterospin system, a field-induced antiferromagnetic to canted-spin antiferromagnetic phase was observed, similar to that observed here [11].

4. Supplementary material

Crystallographic data for the structural analysis have been deposited with the Cambridge Crystallographic Data Centre, CCDC No. 195541. Copies of this information may be obtained free of charge from The Director, CCDC, 12 Union Road, Cambridge, CB2 1EZ, UK (fax: +44-1223-336033; e-mail: deposit@ccdc.cam.ac.uk or http://www.ccdc.cam.ac.uk).

5. Note added in proof

Complex **1**·HOAc·H_2O has recently been reported but with a much less detailed magnetic study then that provided here [27].

Acknowledgements

This work was supported by an ARC Large Grant (to K.S.M.), an ARC Fellowship (to S.R.B.) and a Sir J. McNeill scholarship (to D.J.P.). We thank Professors T. Mallah and M. Kurmoo for valuable discussions.

References

[1] O. Kahn, Molecular Magnetism (Chapter 12), VCH, New York, 1993.
[2] O. Kahn, Adv. Inorg. Chem. 43 (1995) 179.
[3] P. Day, A.E. Underhill (Eds.), Metal-organic and Organic Molecular Magnets, Phil. Trans. R. Soc. London A. 357 (1999) see articles therein.
[4] K.R. Dunbar, R.A. Heintz, Prog. Inorg. Chem. 45 (1997) 283.
[5] V.I. Ovcharenko, R.Z. Sagdeev, Russ. Chem. Rev. 68 (1999) 345.
[6] M. Verdaguer, A. Bleuzen, C. Train, R. Garde, F.F. De Biani, C. Desplanches, Philos. Trans. R. Soc. London, Ser. A 357 (1999) 2959.
[7] S.R. Batten, P. Jensen, C.J. Kepert, M. Kurmoo, B. Moubaraki, K.S. Murray, D.J. Price, J. Chem. Soc., Dalton Trans. (1999) 2987.
[8] M. Kurmoo, C.J. Kepert, New J. Chem. 22 (1998) 1515.
[9] J.S. Miller, J.L. Manson, Acc. Chem. Res. 34 (2001) 563.
[10] G. De Munno, W. Ventura, G. Viau, F. Lloret, J. Faus, M. Julve, Inorg. Chem. 37 (1998) 1458.
[11] V.N. Ikorskii, V.I. Ovcharenko, Y.G. Shvedenkov, G.V. Romanenko, S.V. Fokin, R.Z. Sagdeev, Inorg. Chem. 37 (1998) 4360.
[12] H.-L. Sun, B.-Q. Ma, S. Gao, G. Su, J. Chem. Soc., Chem. Commun. (2001) 2586.
[13] X. Ren, Y. Chen, C. He, S. Gao, J. Chem. Soc., Dalton Trans. (2002) 3915.
[14] K. Van Langenberg, S.R. Batten, K.J. Berry, D.C.R. Hockless, B. Moubaraki, K.S. Murray, Inorg. Chem. 36 (1997) 5006.
[15] D.J. Price, S.R. Batten, B. Moubaraki, K.S. Murray, J. Chem. Soc., Chem. Commun. (2002) 762.
[16] G. Longo, Gazz. Chim. Ital. 61 (1931) 575.
[17] T. Sala, M.V. Sargent, J. Chem. Soc., Chem. Commun. (1978) 253.
[18] Z. Otwinowski, W. Minor, Meth. Enzymol. 276 (1997) 307.
[19] G.M. Sheldrick, SHELX 97, Program for Crystal Structure Refinement, University of Göttingen, Göttingen, Germany, 1997.
[20] H. Kumagai, C.J. Kepert, M. Kurmoo, Inorg. Chem. 41 (2002) 3410.
[21] B.J. Kennedy, K.S. Murray, Inorg. Chem. 24 (1985) 1552.
[22] S.J. Blundell, Magnetism in Condensed Matter (Chapter 5), Oxford University Press, Oxford, 2001.
[23] A.K. Gregson, N.T. Moxon, Inorg. Chem. 20 (1981) 78.
[24] A.K. Gregson, P.C. Healy, Inorg. Chem. 17 (1978) 2969.
[25] A. Marvilliers, S. Parsons, E. Riviere, J.-P. Audiere, M. Kurmoo, T. Mallah, Eur. J. Inorg. Chem. (2001) 1287.
[26] A.J. Edwards, B.F. Hoskins, R. Robson, J.C. Wilson, B. Moubaraki, K.S. Murray, J. Chem. Soc., Dalton Trans. (1994) 1837.
[27] A.J. Tasiopoulos, N.C. Harden, K.A. Abboud, G. Christou, Polyhedron 22 (2003) 133.